Journal of Environment and Earth Science
ISSN 2224-3216 (Paper) ISSN 2225-0948 (Online)
Vol.8, No.5, 2018

Seismic Response Analysis of Underground Structures

Koram Samuel Sakyi [1*] Korankye Benjamin [2] Kweitsu Godson[2]
1.School of Civil Engineering and Mechanics, Jiangsu Univeristy, PO box 321, Zhenjiang, China
2.School of Management and Economics, Jiangsu University, PO box 321, Zhenjiang, China

Abstract
The development and utilization of underground space becomes a new era hot issue for civil engineering in the 21st century. Among them, the subway is one of the mean vehicles of people's daily travel, and the seismic performance requirements for its structure is particularly high. In this paper, the real river-crossing subway shield tunnel is the research object, A detailed introduction has made to the river-crossing tunnel model: the meshing, the seismic load input and boundary conditions, material constitutive model. Then, the pseudo-static method and FLAC3D are used to analyze the seismic response of the river-crossing tunnel model, meanwhile, considering a certain dynamic magnification coefficient to reflect the dynamic response of underground structures. In addition, this paper analyzes the river-crossing tunnel does or does not consider the condition of water. Through the above analysis, this paper gets the following conclusions: (1) Under the effect of transverse shear wave, the transverse displacement of the tunnel is bigger, the vertical displacement is smaller; (2) Under the effect of transverse shear wave, the transverse relative displacement at the tunnel top and bottom is the largest. (3) under the seismic action effect, the tunnel has certain residual deformation. Considering the groundwater effect, there are the following conclusions of the river-crossing tunnel: (1) the surface of the soil is quite close from the permeable boundary, pore water pressure dissipation more easily, soil pore water pressure is not easy to dissipate in the depths; (2) The effective stress decreased with the accumulation of pore water pressure; (3) After the earthquake, void water pressure dissipates, effective stress increase.
Keywords: Earthquake damage, underground structure, river-crossing tunnel, dynamic response.

1. Introduction

Human use of underground space has a long history, the use of the purpose and form are numerous. In today's era of rapid urban development, underground space in the expansion of urban space, ease the pressure of urban traffic and other aspects of its unique superiority. Therefore, the development of urban underground space is rapid.

According to H. Takasaki (2000), the International Conference on Urban Underground Space, held in Tokyo in 1991, adopted the "Oriental Declaration", which proposed that the 19th century was the century of the bridge, the twentieth century was the century of high-rise buildings, and the 21st century was the century of "underground space". Japan in this opportunity, underground space planning, construction and legislation and other aspects of the rapid development of Japan in the late 1950s to the early 1970s had a large-scale development of the use of shallow underground space, to the late 80s.The development and utilization of deep underground space of 50 ~100m has been studied. Others such as the United States and other European and American countries underground space development and utilization is also developing rapidly.

An article published by Nikolai Bobylev (September, 2010) denotes that; in China, the development and utilization of underground space began with the needs of civil air defense. Until the past decade, with the rapid development of China's economy, the subway construction has seen an exorbitant development, to the city subway station as the center, along the underground shopping malls, underground commercial street and other urban underground complex have emerged, to promote the Chinese city underground space Development and utilization of the climax, China has entered the subway project construction of the golden age, China's urban underground space development and utilization also ushered in the rapid development period. Wuhan subway construction is in the ascendant, but also to promote the rapid development of underground space in Wuhan, and the development potential is huge.

With reference to the publication of Cilingir U et al (2010), underground structure such as subway station is an important part of lifeline engineering, which is a good place for earthquake avoidance and evacuation. Its seismic problem has become an important part of seismic engineering and disaster prevention and mitigation of urban engineering. Due to the small number of early underground structures and the lack of importance, the destruction of underground structures caused by earthquakes did not attract people's attention, thus forming the wrong concept of underground structure in the earthquake, thus ignoring the underground structure of the earthquake design. However, the fact that the Kobe City subway station and the intervening tunnel had been severely damaged in the 1995 Hanshin earthquake had brought great impact to this traditional concept, which attracted the great attention of many earthquake workers. The Hanshin earthquake clearly shows that there may be serious damage to the underground structure such as the subway and other parts of the strata where the deformation and displacement may occur. Before the Hanshin Earthquake in Japan in 1995, there were reports of

damage to earthquakes due to the damage to earthquakes and the structure of small water supply systems in the past earthquakes. However, reports on earthquakes were rare and less damaging. As in the 1976 Tangshan earthquake (ML7.8), the newly built Tianjin subway has been tested by the earthquake (Tianjin earthquake intensity of 7 to 8 degrees), only in the sinking site of the surface layer of local shedding or cracks the signs, but did not find significant damage. Another example is the 1985 earthquake (ML8.1), a section built in the soft foundation of the box-shaped subway tunnel, in the transition from the basement to the upper section of the transition zone, the seams scattered parts; another section is shield In the advancement of the sewer tunnel, the longitudinal connecting bolts in the part connected to the working shaft are cut, and longitudinal cracks are formed at the top of the other end of the tunnel, and the concrete in the joint part of the tunnel pipe is dislocated. Kobe earthquake, the excavation tunnel damage is more serious, shield tunnel damage is very slight. More than 90% of the sections of the 900m interval tunnel between the large open station and the new station have a crack along the line in the left and right sides of the wall, and there is a water leakage phenomenon. But the shield tunnel was put into operation soon after the earthquake, indicating that: relative to the subway station, the shield tunnel damage less light.

A report by Huan-Qing Li et al (September, 2013) on an integrated planning concept for the emerging underground urbanism indicated that the seismic characteristics show the strength of the connecting bolts and the flexibility of the waterproofing layer are the key factors for the seismic performance of the shield tunnel. At the same time, it should be eminent that the strength of the segment connection is reduced due to corrosion and aging. In addition, for steel segments, consideration should also be given to how to deal with the problem of mismatches between the lining concrete, and some scholars recommend the use of reinforced concrete as secondary lining.

Wuhan City, the current urban earthquake disaster prevention planning has been implemented for more than 15 years, cannot meet the requirements of rapid urban development. Wuhan City People's Government agreed that the Wuhan Urban and Rural Construction Committee from the end of 2008 began to start the Wuhan earthquake disaster prevention planning preparation work. Wuhan City, although not a strong earthquake area, but vulnerable to the impact of foreign earthquakes, such as 2005, Jiangxi Jiujiang 5.7 earthquake, Wuhan city earthquake obvious. At the same time, in 2006, Wuhan City was listed as one of the eleven national key fortification cities that could have occurred more than fortified earthquakes. In addition, large-scale underground space construction is nearly 20 years to appear, most have not been tested by the earthquake, catastrophic earthquake damage record, thus ignoring the underground space structure of the earthquake problem. (ATC (2016). Tentative Provisions for the Development of Seismic Regulations for Buildings. Applied Technology Council Report, ATC 3-06, Palo Alto, California.)

An article by Xuepeng Zhang, et al (January 2018) connotes that at contemporaneous, most researches on seismic resistance of metro are engrossed on computational theory and calculation methods, and the dynamic response of concrete structure under given ground motion is calculated and analyzed. But in the dynamic response, the structure is safe, whether it has been destroyed, that is, structural safety assessment of the study has not been reported. Japan is an earthquake-prone country, while Japan's underground space development is also the most developed. In 1995, the Kobe earthquake in Japan caused great damage to the underground structures such as subway stations and intervening tunnels. As a turning point, combined with the most serious devastation in the Kobe earthquake, Japanese scholars studied the seismic analysis theory and design method of underground structures A lot of research. Huo and others in the research results for the first time using the relative displacement of the column relative to the height of the column as an evaluation index to evaluate the seismic performance of the underground structure.

The earliest method of seismic analysis was made by Professor Dasen Sumeri, Japan, before the 1950s. The design method is mainly based on the inertial force multiplied by an empirical coefficient, the method is easy to operate, at the time has been widely respected in the early 1960s, the former Soviet scholar Fodieva estimated the structure in each of the various combinations of pressure-pull waves and shear waves in any direction of the cross section of the structure May be the most unfavorable state on the basis of the earthquake under the action of the underground structure of the security of the proposed a general solution. At the same time, Newmark et al. proposed a free-field deformation method, which applies the deformation of various free-field structures under earthquake action directly to structural deformation. The BART design guidelines for the subway in the San Francisco Bay Area in 1969 and the SCETD design guidelines used in the design of the Los Angeles Mass Transit Railway in 1990 belonged to this law. In the late 1970s, Japanese scholars used seismic observation data as the starting point, clear for the underground structure plays a decisive role in the surrounding geotechnical deformation, rather than inertia. And the mathematical model is established by field observation and model test. Combined with the theory of fluctuation, the response displacement method of seismic response analysis of underground structure cross section is proposed. In the 1980s, American scholar Shukla based on the principle of elastic foundation beam, the tunnel-ground soil interaction is equivalent to quasi-static problem. In the same period, the American scholar Dasgupta proposed a recursive diffraction method by establishing a dynamic

impedance matrix in the cross-section.

A case report by Yu Miao, et al (2018) presages that with the improvement of the seismic analysis method of underground structures, many scholars have turned to the influence factors of underground structure response under earthquake action. Hashash also pointed out that the greater the depth of the tunnel, the more difficult the tunnel. Ulas Cilingir et al. explored the effects of the input seismic waves on the seismic response of the tunnel and the effect of depth on the seismic response of tunnels with different cross sections. Cheng-Hsun Chen et al. studied the seismic damage mechanism of different depth tunnels, and pointed out that when the tunnel depth is one quarter of the wavelength, the increase of the internal force caused by the earthquake will be very obvious.

In this paper, the effects of parallel tunnel spacing, lining thickness and material properties on the seismic response of subway shield tunnel are analyzed by FLUSH in the study of the influence factors of tunnel seismic response. Kong Wei et al. studied the effects of different structures and joint parameters on the seismic response of the tunnel and the damping effect of the foundation reinforcement. Liu Guanglei et al. simulated the seismic response of subway tunnels in liquefiable soil by finite element program DIANA SWANDYEE. Wang Guobo et al. studied the seismic performance of the adjacent porous tunnel, and pointed out that the tunnel spacing has no significant effect on the tunnel seismic response and the 4-hole vertical cross tunnel is better than the 4-hole parallel overlapping tunnel.

With this, the researcher will use quasi - static method to analyze the seismic response of the tunnel through FLAC3D, and the dynamic response of the underground structure is considered by considering the dynamic amplification coefficient. (Building Seismic Safety Council (BSSC) (2016a)).

Under the premise of understanding the seismic response of the underground structure and the commonly used method of seismic analysis of the underground structure, the basic principle and related steps of the quasi - static calculation method are grasped, and the calculation points of the quasi - static calculation method and the dynamic calculation method are summarized. Calculate the seismic response of shield tunneling. While requiring consideration of the effects of groundwater. (Building Seismic Safety Council (BSSC) (2016a))

2.0 Seismic Response Calculation and Analysis Example of River Crossing Tunnel (Without Consideration of Groundwater)

2.1 Calculated regions and meshes

In order to reduce the interference of the reflected wave on the artificial boundary surface, it can increase the calculation range and use the damping of the soil to dissipate the reflected wave, but the calculation range is too large to increase the calculation time and reduce the working efficiency. Therefore, the selection of the calculation range must be reasonable, it is necessary to reduce the artificial boundary of the reflected wave interference, and will not significantly increase the calculation time.

According to the study of Professor Lou Menglin, it is shown that the ratio of the size of the foundation plane to the dimension of the structural plane is greater than 5, the result of the dynamic calculation can be stabilized and the influence of the lateral boundary can be neglected. According to the results of Chen Yueqing, the influence of the lateral boundary can be neglected when the ratio of the free-field plane dimension to the width of the model structure is greater than 2. Project member Wang Guobo also studied the calculation of the calculation range of dynamic analysis.

For the typical subway station structure in engineering practice, combined with the above research results, the calculation width along the horizontal excitation direction is taken as 5 times than the width of the station structure (that is, the left and right sides of the soil are two times than the width of the station).

For the horizontal input of the seismic wave, the calculation shows that: the vertical calculation of the length of the station takes as the longitudinal length of 2 times, 4 times, 6 times the width of the horizontal station (that is, before and after the soil take the station lateral span of 1 times, 2 times, 3 times, the difference between the calculated results are within 10%. Considering the applicability of the method (considering the longitudinal seismic resistance of the structure) and the reasonable calculation speed, the selection of the longitudinal calculation length is consistent with the selection of the horizontal calculation length, and the width of the station structure is twice than the width of the station.

According to the Wuhan Yangtze River Tunnel Engineering Geotechnical Investigation Report, the bedrock surface is taken as 50m underground.

According to the selection principle of the above calculation range, the calculation range is selected as: 90 (horizontal) × 100 (horizontal vertical) m × 50m (vertical). The calculation model is shown in Figure 1 ~ 2.

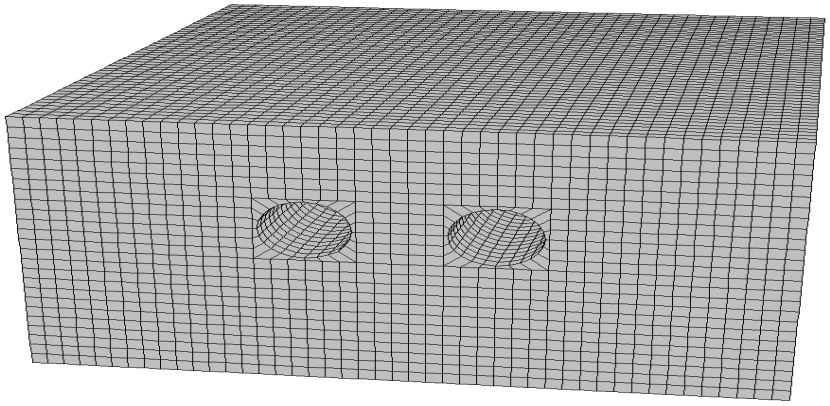

Fig.1 The diagram of Calculated model

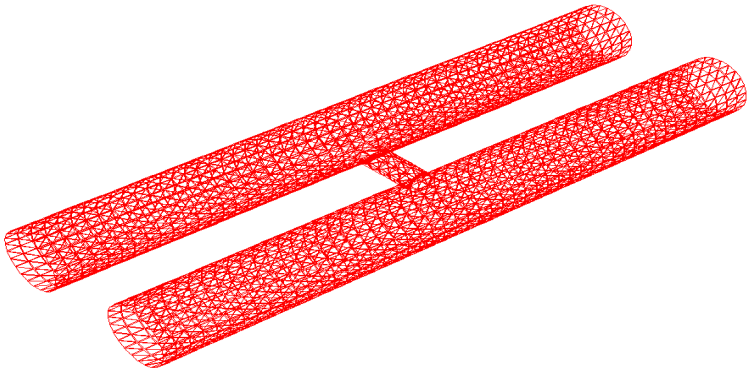

Fig.2 Model diagram of tunnel structure calculation

2.1.1 Input of seismic load

In the dynamic calculation, the earthquakes and earthquakes with 10% and 2% overturning probability over the next 50 years are calculated at the ground 50 m bedrock. The peak of large earthquake acceleration is twice the acceleration peak. The time-course and spectral characteristics of the earthquake acceleration are considered in Fig. 3 and Fig. 4 when considering these three kinds of working conditions. Among them, according to the "Building Seismic Design Code" requirements: for the 8-degree seismic fortification structure, taking into account the impact of vertical earthquakes, the amplitude of the corresponding level of ground motion acceleration of 2 /3.

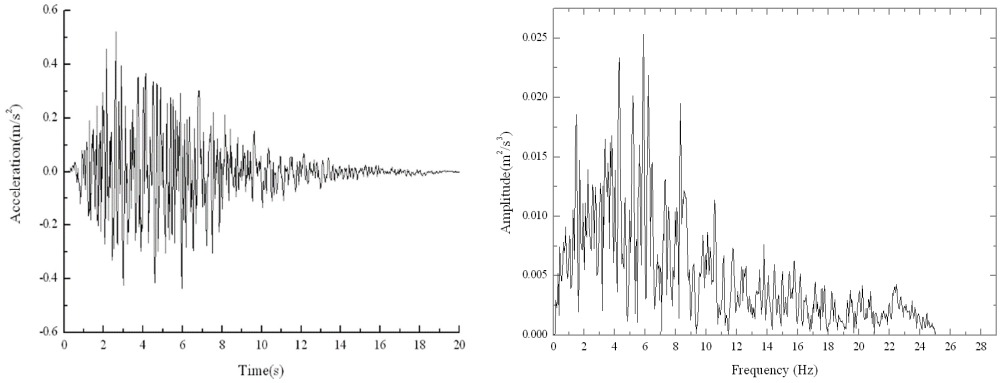

Fig.3 Curve of time history and spectrum of Wuhan artificial seismic wave at 50 meters underground in the next 50 years over 10% probability

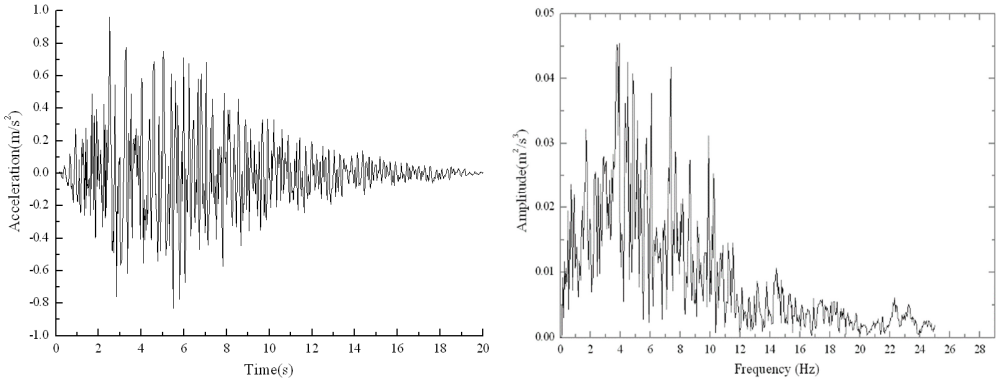

Fig.4 Curve of time history and spectrum of Wuhan artificial seismic wave at 50 meters underground in the next 50 years over 2% probability

2.1.2 Constitutive model of material

The results show that the three-parameter Davidenkov model can be used to fit the experimental results well. In this paper, the Davidenkov model is used to simulate the nonlinear characteristics of Wuhan soft soil, and the dynamic stress-strain relationship of soft soil can be described by Davidenkov model. The Davidenkov model can be described as:

Error! Objects cannot be created from editing field codes. （2-3）

Error! Objects cannot be created from editing field codes. （2-4）

Where A, B and γ_r are the fitting constants, γ_r is also the reference shear strain, γ_d is the instantaneous shear strain, G_d and λ are the instantaneous shear modulus and damping ratio, G_{max} and λ_{max} are the maximum dynamic shear Amount and maximum damping ratio. When A = 1 and B = 0.5, the Davidenkov model degrades into the common Hardin-Drnevich model.

Literature On the basis of experimental study, four common soils in Wuhan soft soil are given: the model parameters of silty clay, clay, silt and sand (Table 1).

Table 1 Davidenkov model parameters for four soil types

Soil type	G_d				Λ	
	A	B	$\gamma_r(10^{-4})$	Correlation coefficient R	β	Correlation coefficient R
Silty clay	1.2046	0.4527	7.1	0.9987	1.3185	0.9815
Clay	0.5773	0.6487	20.4	0.9954	1.3690	0.9814
Silt	0.6909	0.5530	15.5	0.9994	1.2468	0.9796
sand	0.8094	0.5421	13.5	0.9994	1.0735	0.9952

The Davidenkov model is used to describe the nonlinear characteristics of soft soil. The calculation parameters of soil are shown in Table 2.

Table 2 Calculation parameters of soil

Soil layer	Severe (KN/m^3)	Shear speed (m/s)	Poisson's ratio
Silty clay	19.6	186	0.4
Silt	19.8	182	0.35
Fine sand	20.1	263	0.32
Fine sand	20.1	294	0.32
In the coarse sand	20.5	358	0.3

For the reinforced concrete, the elastic model is used for the static calculation. The M-C model is used in the dynamic calculation to consider the nonlinear deformation of the concrete.

2.2 Static calculation results and analysis

Static load to consider the load when the soil and the structure of the weight and ground overload, ground overload according to the standard take 20kPa. Due to the symmetry of the structure, this report only analyzes the stress and deformation of the left tunnel and the communication channel. The bending curve of the tunnel along the longitudinal direction shown in Figure 5, contact channel bending Figure 6, the structure of the stress cloud shown in Figure 7.

As can be seen from Figures 5 to 7:

1, the bending moment of the tunnel is larger, the contact path of the bending moment is small, they have stress concentration at the junction;

2, the top and bottom of the tunnel bending moment is positive, left arch waist and right arch bending

moment is negative, indicating the top and bottom of the tunnel at the bottom of the tube surface tension, in the left arch and the arch at the arch Outer surface tension;

3, along the tunnel longitudinal about 50m, due to the tunnel right arch and contact channel phase, so there is a sudden change in bending moment.

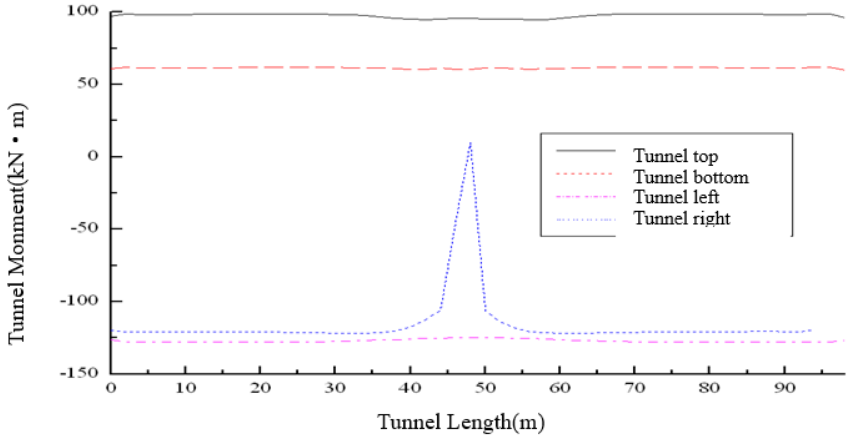

Fig.5 Curve of tunnel bending moment along the longitudinal direction

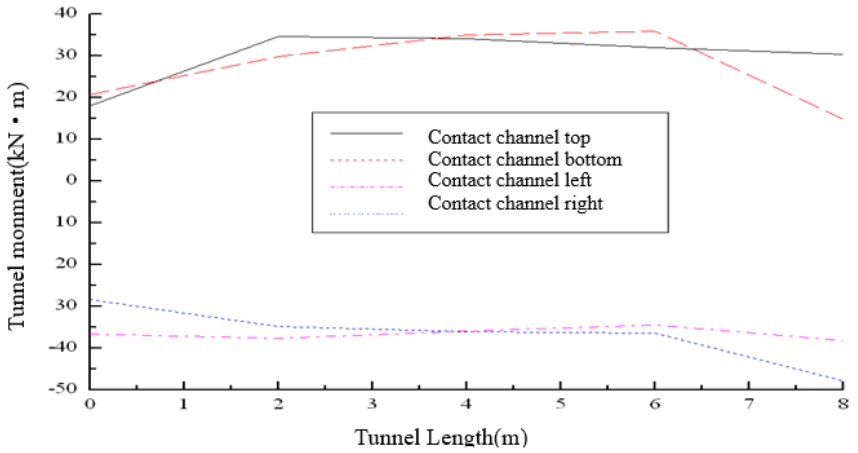

Fig. 6 Curve change curve along the longitudinal channel of the contact channel

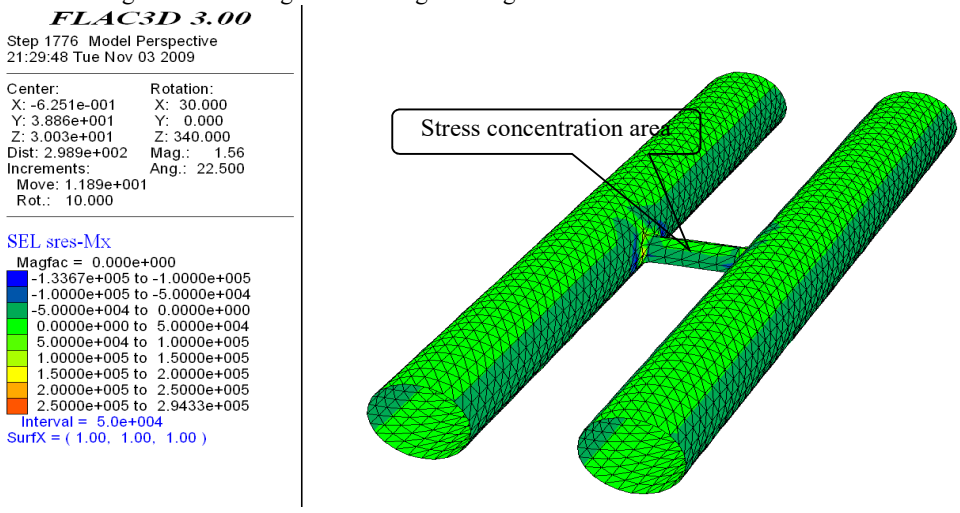

2.3 Structural dynamics analysis

A combined force of the subway station structure in the static and surpassing probability of 10% and 2% and the

Wuhan artificial wave was understudy. The purpose of the analysis is to find out the most unfavorable parts of the force of the structure, to test the seismic stability of the structure, and to compare the internal forces of the most unfavorable parts of the structure with the static internal forces of the corresponding parts. The seismic load is the most unfavorable Site of the internal force increase, so that engineering practice reference application. The calculation of internal force increase caused by seismic load is:

2.3.1 Seismic response analysis of structures at middle earthquake

2.3.1.1 force analysis

Respectively, consider the tunnel and the contact channel and their junctions in the mid-level seismic load under the earthquake moment and its increase in the maximum bending moment of the tunnel section along the longitudinal curve shown in Figure 8, the tunnel in the static and joint action Bending moment and bending moment increase in Table 3, 4, contact channel in the static and resultant force under the bending moment and bending moment increase in Table 5,6, tunnel and contact channel junctions in the static and joint action Moment and moment increase in Table 7. From Figure 8 and Table 3 to 7 we can see:

1, compared with Figure 5,8, the tunnel in the static and dynamic role along the tunnel longitudinal bending moment of the same trend;

2, The average increase of bending moment is 213%, the average increase of tunnel bending moment is 34.7%, and the average increase of contact moment is 48.7%.

3, although the contact channel of the increase in bending moment, but the bending moment compared to the river tunnel is much smaller;

4, in the cross-river tunnel and the junction of the existence of stress concentration phenomenon, need to pay attention.

Table 3 tunnel top, bottom in the static and resultant force under the bending moment and bending moment increase

Length of tunnel longitudinal (m)	Tunnel top moment (KN*m)				Bend at the bottom of the tunnel (KN*m)			
	Static	Composition of forces	Increased amplitude (%)	Average increase in amplitude (%)	Static	composition of forces	Increased amplitude (%)	Average increase in amplitude (%)
0	97.146	168.46	73.41		60.7	73.093	20.42	
2	98.575	170.79	73.26		61.827	74.965	21.25	
4	98.399	168.42	71.16		61.621	73.65	19.52	
6	98.34	162.81	65.56		61.576	71.824	16.64	
8	98.364	157.49	60.11		61.588	71.254	15.69	
10	98.385	154.08	56.61		61.59	71.706	16.42	
12	98.426	150.52	52.93		61.598	72.085	17.02	
14	98.474	145.29	47.54		61.611	72.403	17.52	
16	98.52	139.26	41.35		61.634	72.536	17.69	
18	98.572	135.16	37.12		61.657	72.608	17.76	
20	98.628	133.11	34.96		61.688	72.612	17.71	
22	98.675	131.41	33.17		61.71	72.338	17.22	
24	98.705	129.36	31.06		61.736	72.197	16.94	
26	98.688	127	28.69		61.756	72.106	16.76	
28	98.605	124.82	26.59	39.8	61.757	72.37	17.19	20.8
30	98.41	124.87	26.89		61.728	72.97	18.21	
32	98.063	123.98	26.43		61.647	73.148	18.66	
34	97.521	122.29	25.40		61.48	72.446	17.84	
36	96.772	120.54	24.56		61.207	71.993	17.62	
38	95.876	118.63	23.73		60.821	72.2	18.71	
40	95.063	116.27	22.31		60.437	73.018	20.82	
42	94.786	113.55	19.80		60.57	75.196	24.15	
44	95.315	114.38	20.00		61.337	79.21	29.14	
46	95.887	115.44	20.39		60.314	82.233	36.34	
48	95.489	114.35	19.75		60.356	81.731	35.41	
50	94.959	113.63	19.66		61.51	84.928	38.07	
52	95.229	112.93	18.59		61.653	83.087	34.77	
54	94.979	113.43	19.43		60.93	78.079	28.15	
56	94.496	116.11	22.87		60.616	74.972	23.68	
58	94.86	119.12	25.57		60.794	73.71	21.25	

60	95.781	121.54	26.89	61.11	73.009	19.47	
62	96.762	123.41	27.54	61.379	73.002	18.94	
64	97.57	126.37	29.52	61.567	73.542	19.45	
66	98.138	129.54	32.00	61.67	73.706	19.52	
68	98.486	131.05	33.06	61.723	73.327	18.80	
70	98.667	131.34	33.11	61.746	72.993	18.21	
72	98.741	131.55	33.23	61.741	72.869	18.02	
74	98.746	131.36	33.03	61.719	72.724	17.83	
76	98.706	132.01	33.74	61.704	72.774	17.94	
78	98.647	134.25	36.09	61.683	72.78	17.99	
80	98.58	136.26	38.22	61.655	72.431	17.48	
82	98.517	138.99	41.08	61.641	72.294	17.28	
84	98.468	143.82	46.06	61.621	72.211	17.19	
86	98.424	149.35	51.74	61.612	72.28	17.31	
88	98.388	154.25	56.78	61.602	72.808	18.19	
90	98.366	159.63	62.28	61.596	73.915	20.00	
92	98.351	165.54	68.32	61.568	75.946	23.35	
94	98.46	170.61	73.28	61.674	77.13	25.06	
96	98.516	175.4	78.04	61.848	77.408	25.16	
98	96.194	178.59	85.66	59.981	75.905	26.55	

Table 4 Tunnel two arch in the static and force under the bending moment and bending moment increase

Longitudinal length (m)	Tunnel left arch bending moment (KN*m)				Tunnel right arch bending moment (KN*m)			
	Static	Composition of forces	Increased amplitude (%)	Average increase in amplitude (%)	Static	compositi on of forces	Increased amplitude (%)	Average increase in amplitude (%)
0	-126.32	-191.25	51.40		-119.86	-176.41	47.18	
2	-127.93	-194.41	51.97		-120.91	-174.75	44.53	
4	-127.71	-193.32	51.37		-120.81	-171.8	42.21	
6	-127.66	-190.4	49.15		-120.71	-169.8	40.67	
8	-127.68	-187.73	47.03		-120.71	-168.75	39.80	
10	-127.7	-184.58	44.54		-120.72	-169.89	40.73	
12	-127.71	-182.1	42.59		-120.75	-171.61	42.12	
14	-127.74	-181.94	42.43		-120.78	-172.33	42.68	
16	-127.76	-182.03	42.48		-120.83	-171.35	41.81	
18	-127.78	-180.06	40.91		-120.9	-169.49	40.19	
20	-127.8	-177.22	38.67		-120.99	-168.07	38.91	
22	-127.81	-175.93	37.65		-121.09	-167.12	38.01	
24	-127.8	-176.29	37.94		-121.22	-166.96	37.73	
26	-127.76	-176.52	38.17		-121.36	-168.17	38.57	
28	-127.68	-175.19	37.21		-121.52	-169.3	39.32	
30	-127.53	-172.25	35.07	38.2	-121.66	-169.79	39.56	40
32	-127.32	-168.74	32.53		-121.75	-169.77	39.44	
34	-127.01	-166.33	30.96		-121.69	-168.94	38.83	
36	-126.64	-165.19	30.44		-121.32	-167.67	38.20	
38	-126.21	-164.58	30.40		-120.25	-166.87	38.77	
40	-125.78	-163.79	30.22		-117.64	-164.78	40.07	
42	-125.4	-163	29.98		-112.5	-160.69	42.84	
44	-125.12	-162.95	30.23		-106.11	-148.83	40.26	
46	-124.94	-162.51	30.07		-45.276	-71.043	56.91	
50	-124.89	-159.77	27.93		-106.4	-113.64	6.80	
52	-124.99	-159.67	27.75		-113.91	-137.97	21.12	
54	-125.18	-158.82	26.87		-118.32	-156.68	32.42	
56	-125.47	-157.88	25.83		-120.75	-163.9	35.73	
58	-125.85	-159.08	26.40		-121.62	-167.17	37.45	
60	-126.26	-160.94	27.47		-121.88	-168.4	38.17	
62	-126.67	-162.72	28.46		-121.87	-168.19	38.01	

64	-127.05	-163.89	29.00	-121.75	-167.76	37.79
66	-127.34	-164.78	29.40	-121.59	-167.92	38.10
68	-127.55	-166.74	30.73	-121.42	-168.38	38.68
70	-127.69	-169.85	33.02	-121.26	-168.28	38.78
72	-127.78	-173.73	35.96	-121.13	-167.39	38.19
74	-127.82	-175.05	36.95	-121.02	-167.06	38.04
76	-127.83	-175.75	37.49	-120.92	-168.19	39.09
78	-127.83	-177.45	38.82	-120.85	-170.37	40.98
80	-127.81	-180.09	40.90	-120.8	-171.93	42.33
82	-127.78	-182.74	43.01	-120.75	-173.45	43.64
84	-127.77	-184.94	44.74	-120.72	-175.18	45.11
86	-127.75	-187.82	47.02	-120.69	-175.74	45.61
88	-127.73	-190.2	48.91	-120.66	-175.23	45.23
90	-127.72	-191.4	49.86	-120.7	-175.26	45.20
92	-127.74	-192.23	50.49	-120.92	-173.71	43.66
94	-127.85	-193.02	50.97	-119.47	-170.17	42.44
96	-127.96	-193.92	51.55			
98	-127.08	-191.97	51.06			

Table 5 contact channel at the top, the bottom of the static and dynamic bending moment and bending moment increase

Contact Road longitudinal length (m)	Contact the top of the channel (KN*m)				Contact the bottom of the channel (KN*m)			
	Static	Composition of forces	Increased amplitude (%)	Average increase in amplitude (%)	Static	Composition of forces	Increased amplitude (%)	Average increase in amplitude (%)
0	18.146	33.994	87.34		20.814	41.73	100.47	
2	34.739	46.759	34.60		29.897	41.68	39.40	
4	34.085	44.362	30.15	59.4	34.967	46.73	33.64	61.2
6	31.959	45.223	41.50		35.863	46.48	29.60	
8	30.479	62.02	103.48		14.749	29.91	102.81	

Table 6 contact channel two arch in the static and dynamic bending moment and bending moment increase

Contact Road longitudinal length (m)	Contact channel left arch waist (KN*m)				Contact channel right arch waist (KN*m)			
	Static	Composition of forces	Increased amplitude (%)	Average increase in amplitude (%)	Static	Composition of forces	Increased amplitude (%)	Average increase in amplitude (%)
0	-36.75	-51.977	41.43		-28.384	-44.341	56.22	
2	-37.654	-50.425	33.92		-34.826	-47.71	37.00	
4	-36.005	-47.504	31.94	37.2	-36.169	-48.196	33.25	37.1
6	-34.564	-46.236	33.77		-36.583	-48.556	32.73	
8	-38.295	-55.502	44.93		-47.996	-60.675	26.42	

Table 7 Tunnel and contact channel at the junction of bending moment and bending moment increase

The number of units at the junction	Static	Composition of forces	Increased amplitude (%)	Average increase in amplitude (%)
1	47.111	92.85	97.09	
2	7.4454	52.18	600.78	
3	-29.073	-121.10	316.54	
4	65.188	103.34	58.53	
5	-2.0842	-8.17	292.12	
6	76.131	130.15	70.96	
7	-17.115	-20.11	17.49	
8	65.207	97.35	49.29	213
9	61.369	112.53	83.37	
10	10.313	45.79	344.00	
11	70.367	130.14	84.94	
12	61.325	101.54	65.58	
13	-3.1739	-20.68	551.50	
14	-19.483	-95.65	390.93	
15	48.232	128.89	167.23	

2.3.1.2 Deformation analysis

First, the curve of the maximum lateral displacement of the tunnel along the longitudinal direction (see Fig. 6) is given, and the maximum vertical displacement of the tunnel along the longitudinal direction (see Fig. 11). The contact channel is connected with the tunnel in the longitudinal direction of the tunnel, and the tunnel at this section is selected for deformation analysis. The top, bottom lateral displacement and lateral relative displacement time course of the longitudinal section of the tunnel are shown in Fig. 7. The top and bottom vertical displacements and vertical relative displacements of the tunnel are shown in Figures 8 and 9.

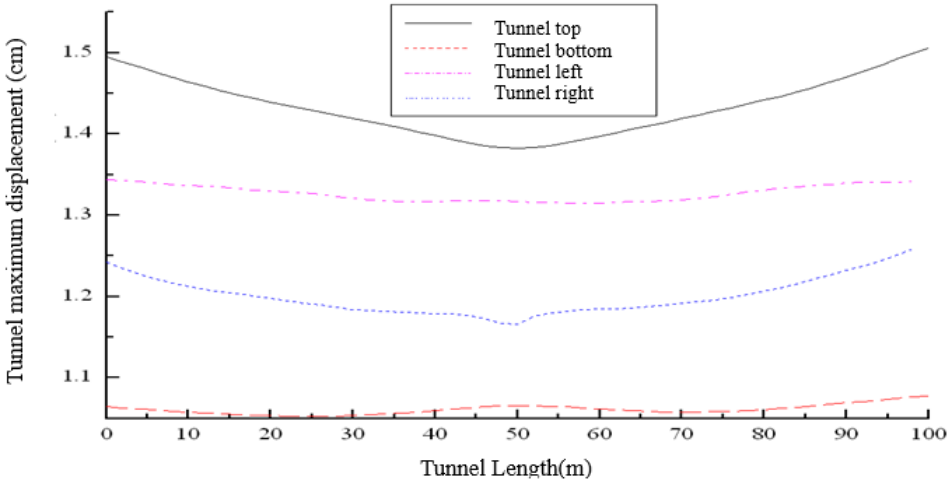

Fig.7 Curve of the maximum lateral displacement of the tunnel along the longitudinal direction

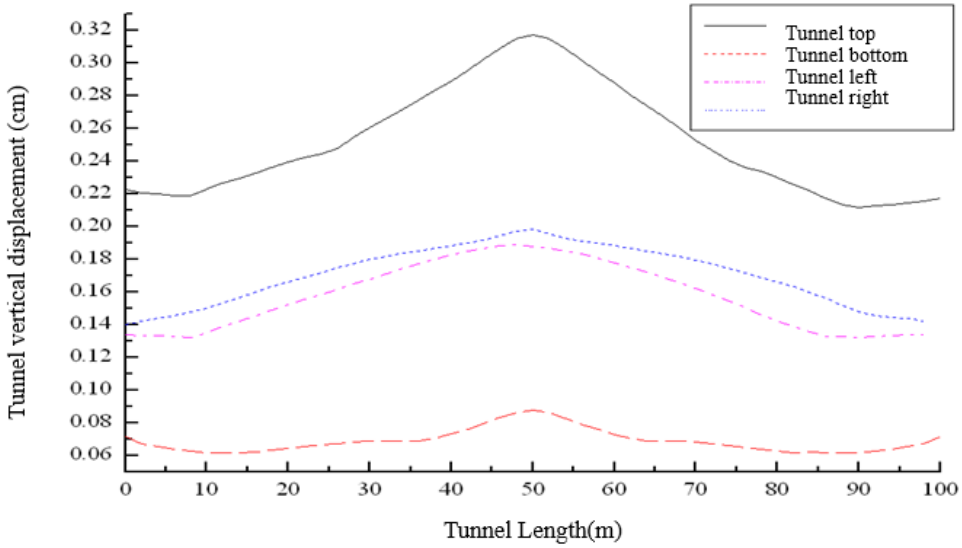

Fig.8 Curve of vertical vertical displacement of tunnel

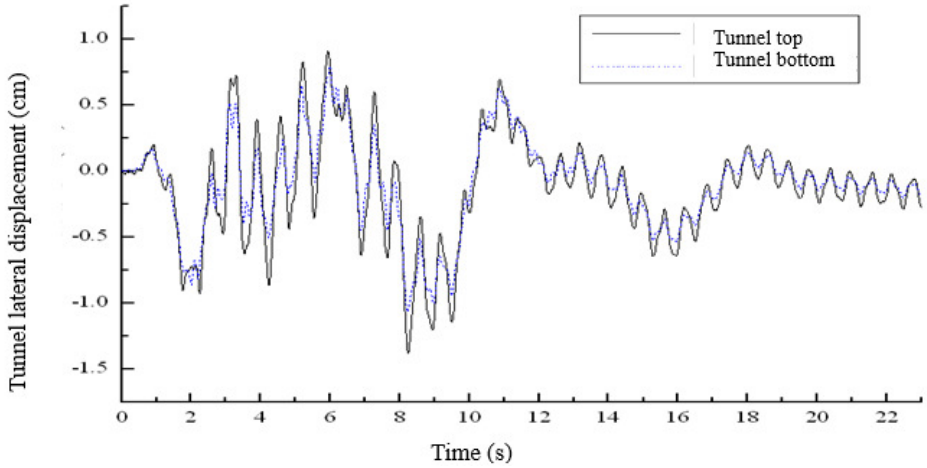

Fig.9 Vertical and horizontal displacement time curves at the top and bottom of the longitudinal section of the tunnel

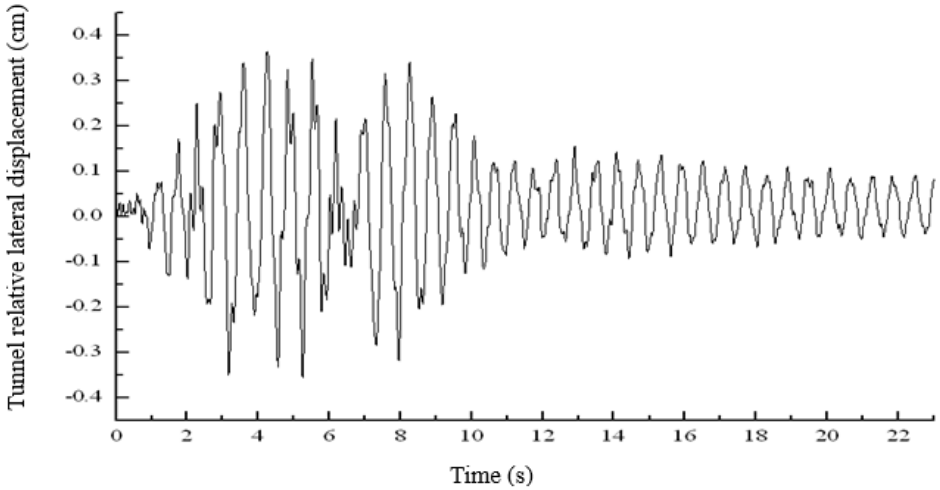

Fig.2-13 Time-dependent curves of the top and bottom transverse displacements in the longitudinal section of the tunnel

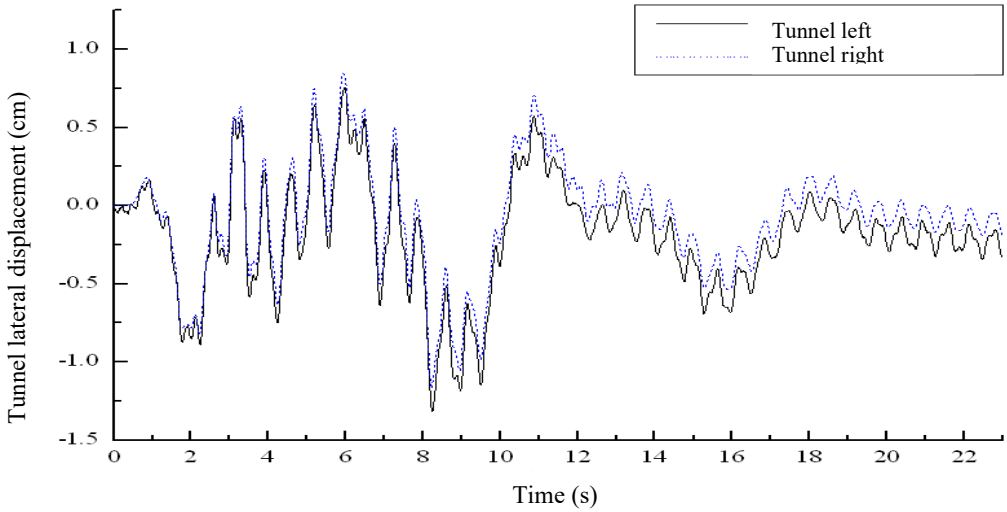

Fig.10 Time-lapse curve of transverse displacement of two arch trenches in longitudinal section of tunnel

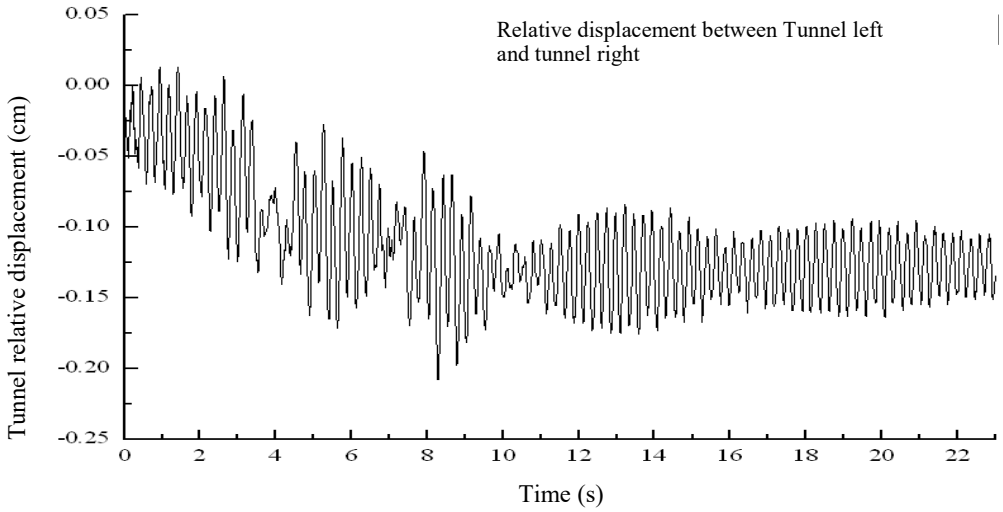

Fig.11 Time-dependent curve of transverse displacement of two arch trenches

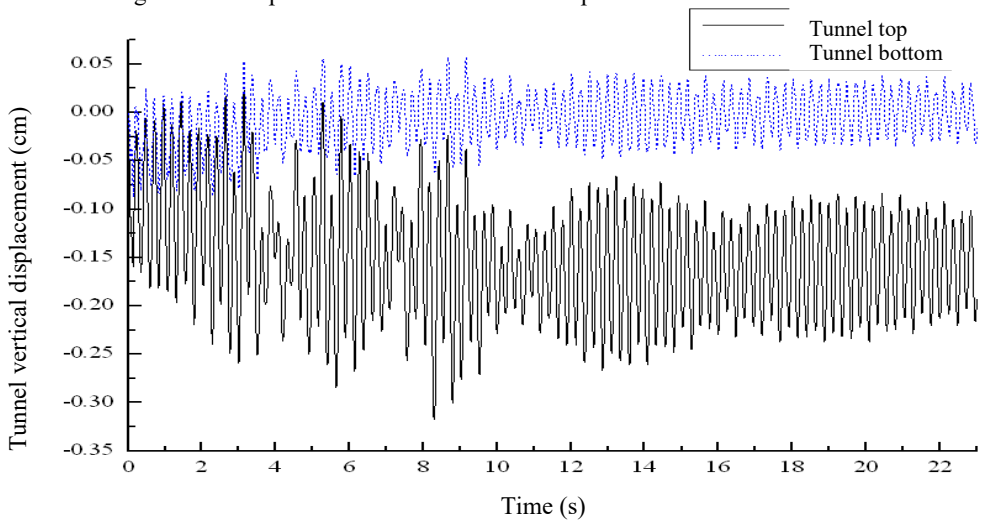

Fig.2-16 Time-history curve of vertical and vertical displacement of the top and bottom of the tunnel

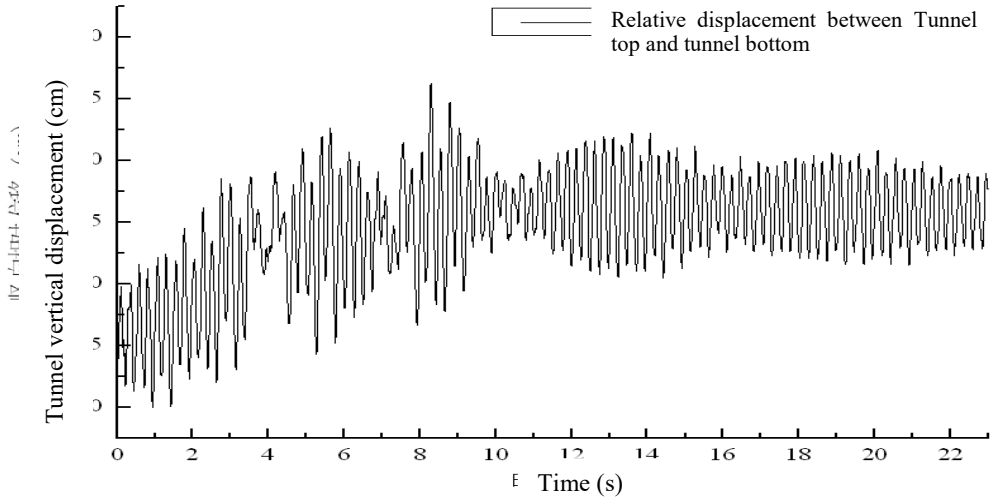

Fig.12 Time-history curve of vertical displacement of the top and bottom of the tunnel in the longitudinal section of the tunnel

From Figures 7 to 12,

1, the lateral displacement of the top of the tunnel is the largest, the lateral displacement of the left arch and the right arch is the second, and the lateral displacement of the bottom is the smallest;

2, The maximum relative displacement of the tunnel at the top and bottom of the tunnel is 0.35cm, and the maximum relative displacement of the tunnel is 0.21cm, and the maximum vertical relative displacement of the top and bottom of the tunnel is 0.26 Cm;

3, under the action of the earthquake, the tunnel has some residual deformation, the relative lateral displacement of the arch of the two arch is 0.13cm, the top of the tunnel, the relative vertical displacement of the bottom is 0.17cm.

2.4.1 Seismic response analysis of structures at large earthquake

2.4.1.1 Force analysis

Respectively, considering the tunnel and the contact channel and their junctions in the earthquake under the level of seismic load and the increase of the moment, the maximum bending moment of the tunnel section along the tunnel longitudinal curve shown in Figure 18, the tunnel in the static and resultant force The bending moment and bending moment increase in Table 8,9, contact channel in the static and joint action under the bending moment and bending moment increase in Table 10,11, tunnel and contact channel junctions in the static and joint force The bending moment is shown in Table 12. From Fig. 18 and Table 8-12,

1, compared with Figure 6,18, the tunnel in the static and dynamic role along the tunnel longitudinal bending moment of the same trend;

2, The average increase of bending moment is 368%, the average increase of tunnel bending moment is 247%, and the average increase of contact moment is 80.3%.

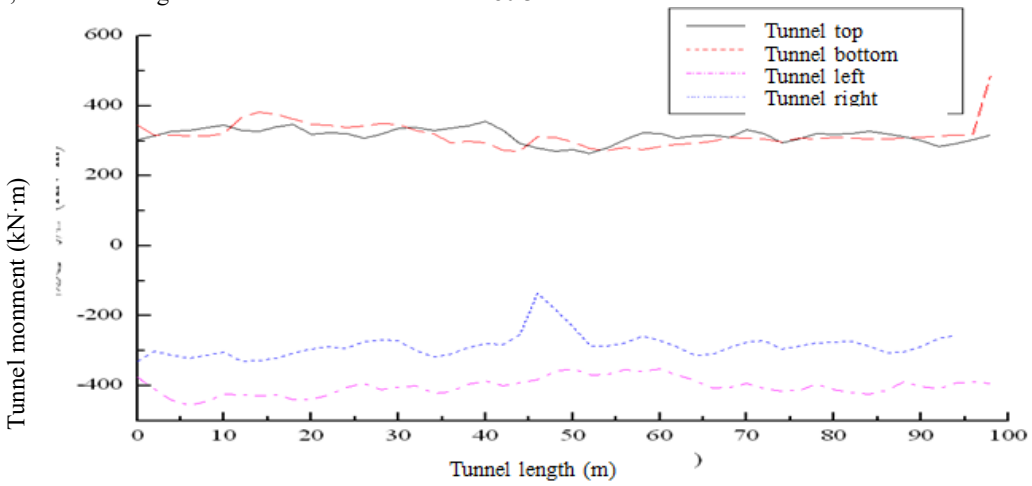

Fig. 13 curve of the maximum bending moment along the longitudinal direction of the tunnel

Table 9 Tunnels at the top and bottom of the tunnel under static and resultant forces

Tunnel longitudinal length (m)	Tunnel top moment (KN*m)				Bend at the bottom of the tunnel (KN*m)			
	Static	composition of forces	Increased amplitude (%)	Average increase in amplitude (%)	Static	composition of forces	Increased amplitude (%)	Average increase in amplitude (%)
0	97.146	302.37	211.25		60.7	344.17	467.00	
2	98.575	314.56	219.11		61.827	317.5	413.53	
4	98.399	327.89	233.22		61.621	316.79	414.09	
6	98.34	329.22	234.78		61.576	313.72	409.48	
8	98.364	339	244.64		61.588	314.05	409.92	
10	98.385	344.96	250.62		61.59	320.81	420.88	
12	98.426	328.92	234.18		61.598	365.91	494.03	
14	98.474	328.23	233.32		61.611	381.09	518.54	
16	98.52	341.48	246.61		61.634	375.28	508.88	
18	98.572	346.85	251.87		61.657	361.44	486.21	
20	98.628	318.26	222.69		61.688	346.11	461.07	
22	98.675	322.03	226.35		61.71	345.05	459.15	
24	98.705	321.14	225.35		61.736	338.97	449.06	
26	98.688	308.62	212.72		61.756	342.17	454.07	
28	98.605	317.94	222.44		61.757	348.87	464.91	
30	98.41	334.99	240.40		61.728	345.87	460.31	
32	98.063	339.21	245.91		61.647	328.76	433.29	
34	97.521	329.78	238.16		61.48	320.3	420.98	
36	96.772	336.71	247.94		61.207	294.66	381.42	
38	95.876	341.7	256.40		60.821	298.7	391.11	
40	95.063	355.85	274.33		60.437	295.28	388.57	
42	94.786	330.22	248.38		60.57	272.67	350.17	
44	95.315	291.48	205.81		61.337	271.75	343.04	
46	95.887	280.07	192.08		60.314	313	418.95	
48	95.489	270.79	183.58	224	60.356	310.86	415.04	417
50	94.959	274.98	189.58		61.51	297.6	383.82	
52	95.229	264.91	178.18		61.653	277	349.29	
54	94.979	279.56	194.34		60.93	273.47	348.83	
56	94.496	303.92	221.62		60.616	281.71	364.75	
58	94.86	322.18	239.64		60.794	275.58	353.30	
60	95.781	321.22	235.37		61.11	283.55	364.00	
62	96.762	308.05	218.36		61.379	291.11	374.28	
64	97.57	313.2	221.00		61.567	291.85	374.04	
66	98.138	316.06	222.06		61.67	299.65	385.89	
68	98.486	310.79	215.57		61.723	309.95	402.16	
70	98.667	331.72	236.20		61.746	308.67	399.90	
72	98.741	321.82	225.92		61.741	304.93	393.89	
74	98.746	294.07	197.80		61.719	297.44	381.93	
76	98.706	306.21	210.22		61.704	308.65	400.21	
78	98.647	320.81	225.21		61.683	306.63	397.11	
80	98.58	318.62	223.21		61.655	309.61	402.17	
82	98.517	320.33	225.15		61.641	306.97	398.00	
84	98.468	327.81	232.91		61.621	305.51	395.79	
86	98.424	320.73	225.87		61.612	305.9	396.49	
88	98.388	312.43	217.55		61.602	307.49	399.16	
90	98.366	301.62	206.63		61.596	310.19	403.59	
92	98.351	283.32	188.07		61.568	313.22	408.74	
94	98.46	291.68	196.24		61.674	315.87	412.16	
96	98.516	304.39	208.98		61.848	318.92	415.65	
98	96.194	315.46	227.94		59.981	487.39	712.57	

Table 10 tunnel two arch in the static and force under the bending moment and bending moment increase

Tunnel longitudinal length (m)	Tunnel left arch bending moment (KN*m)				Tunnel right arch bending moment (KN*m)			
	Static	composition of forces	Increased amplitude (%)	Average increase in amplitude (%)	Static	composition of forces	Increased amplitude (%)	Average increase in amplitude (%)
0	-126.32	-376.15	197.78		-119.86	-329.51	174.91	
2	-127.93	-408.27	219.14		-120.91	-301.82	149.62	
4	-127.71	-441.51	245.71		-120.81	-313.03	159.11	
6	-127.66	-457.18	258.12		-120.71	-321.99	166.75	
8	-127.68	-444.82	248.39		-120.71	-312.72	159.07	
10	-127.7	-424	232.03		-120.72	-303.70	151.57	
12	-127.71	-426.87	234.25		-120.75	-330.69	173.86	
14	-127.74	-428.41	235.38		-120.78	-328.62	172.08	
16	-127.76	-427.34	234.49		-120.83	-322.79	167.14	
18	-127.78	-439.5	243.95		-120.9	-306.83	153.79	
20	-127.8	-439.1	243.58		-120.99	-296.17	144.79	
22	-127.81	-426.21	233.47		-121.09	-289.47	139.05	
24	-127.8	-403.8	215.96		-121.22	-293.99	142.53	
26	-127.76	-393.93	208.34		-121.36	-273.78	125.59	
28	-127.68	-411.28	222.12		-121.52	-270.11	122.28	
30	-127.53	-404.22	216.96		-121.66	-272.18	123.72	
32	-127.32	-400.66	214.69		-121.75	-299.59	146.07	
34	-127.01	-423.38	233.34		-121.69	-316.70	160.25	
36	-126.64	-418.67	230.60		-121.32	-310.04	155.56	
38	-126.21	-395.67	213.50		-120.25	-290.55	141.62	
40	-125.78	-388.38	208.78		-117.64	-281.24	139.07	
42	-125.4	-400.93	219.72		-112.5	-282.05	150.71	
44	-125.12	-391.58	212.96		-106.11	-253.60	139.00	
46	-124.94	-383.92	207.28		-45.276	-135.60	199.50	
50	-124.89	-351.35	181.33	213	-106.4	-232.58	118.59	135
52	-124.99	-368.88	195.13		-113.91	-285.95	151.03	
54	-125.18	-368.24	194.17		-118.32	-287.38	142.88	
56	-125.47	-355.35	183.22		-120.75	-276.96	129.37	
58	-125.85	-359.45	185.62		-121.62	-259.11	113.05	
60	-126.26	-351.86	178.68		-121.88	-272.11	123.26	
62	-126.67	-370.74	192.68		-121.87	-288.95	137.10	
64	-127.05	-384.74	202.83		-121.75	-312.28	156.49	
66	-127.34	-406.07	218.89		-121.59	-309.89	154.86	
68	-127.55	-404.08	216.80		-121.42	-290.39	139.16	
70	-127.69	-393.54	208.20		-121.26	-274.92	126.72	
72	-127.78	-409.85	220.75		-121.13	-271.47	124.11	
74	-127.82	-415.45	225.03		-121.02	-296.11	144.68	
76	-127.83	-412.52	222.71		-120.92	-286.97	137.32	
78	-127.83	-397.27	210.78		-120.85	-277.84	129.90	
80	-127.81	-410.86	221.46		-120.8	-276.90	129.22	
82	-127.78	-421.05	229.51		-120.75	-272.76	125.89	
84	-127.77	-425.48	233.00		-120.72	-287.71	138.33	
86	-127.75	-414.16	224.20		-120.69	-306.48	153.94	
88	-127.73	-389.45	204.90		-120.66	-304.64	152.48	
90	-127.72	-402.77	215.35		-120.7	-288.95	139.40	
92	-127.74	-408.62	219.88		-120.92	-265.20	119.32	
94	-127.85	-391.33	206.09		-119.47	-257.01	115.13	
96	-127.96	-389.36	204.28					
98	-127.08	-392.78	209.08					

Table 11 contact channel at the top, the bottom of the static and dynamic bending moment and bending moment increase

Contact Road longitudinal length (m)	Contact the top of the channel (KN*m)				Contact the bottom of the channel (KN*m)			
	Static	composition of forces	Increased amplitude (%)	Average increase in amplitude (%)	Static	composition of forces	Increased amplitude (%)	Average increase in amplitude (%)
0	18.146	45.311	149.70		20.814	61.78	196.82	
2	34.739	74.051	113.16		29.897	43.28	44.75	
4	34.085	64.116	88.11	123	34.967	46.72	33.62	84
6	31.959	54.791	71.44		35.863	49.87	39.05	
8	30.479	88.819	191.41		14.749	30.50	106.79	

Table 12 contact channel two arch in the static and dynamic bending moment and bending moment increase

Contact Road longitudinal length (m)	Contact channel left arch waist bending moment (KN*m)				Contact channel right cam bending moment (KN*m)			
	Static	composition of forces	Increased amplitude (%)	Average increase in amplitude (%)	Static	composition of forces	Increased amplitude (%)	Average increase in amplitude (%)
0	-36.75	-57.225	55.71		-28.384	-56.92	100.53	
2	-37.654	-65.077	72.83		-34.826	-50.45	44.86	
4	-36.005	-57.073	58.51	60.6	-36.169	-51.05	41.15	54.1
6	-34.564	-50.645	46.53		-36.583	-55.87	52.72	
8	-38.295	-64.839	69.31		-47.996	-62.97	31.18	

Table 13 Joints at the junction of the tunnel and the communication channel

The number of units at the junction	Static (KN*m)	Together (KN*m)	Increase (%)	Average Increase (%)
1	47.111	115.22	144.5713	
2	-29.073	-162.52	459.0066	
3	65.188	117.15	79.71099	
4	76.131	137.87	81.09574	
5	-17.115	-78.47	358.4867	
6	65.207	111.3	70.6872	
7	61.369	128.5	109.3891	368
8	10.313	122.68	1089.567	
9	70.367	175.94	150.032	
10	61.325	122.79	100.2283	
11	-3.1739	-45.32	1327.896	
12	-19.483	-127.54	554.622	
13	48.232	172.66	257.9781	

2.4.1.2 Deformation analysis

First, the curve of the maximum lateral displacement of the tunnel along the longitudinal direction (see Fig. 14) is given, and the maximum vertical displacement of the tunnel along the longitudinal direction (see Fig. 15). The tunnel is connected with the tunnel in the longitudinal direction of the tunnel, and the tunnel at this section is selected for deformation analysis. The tunnel top, bottom lateral displacement and lateral relative displacement time course are shown in Fig. 16 and 17, The lateral displacement and transverse relative displacement time-history curves are shown in Figures 18 and 19. The top and bottom vertical displacements and vertical relative displacements of the tunnel are shown in Figures 20 and 21.

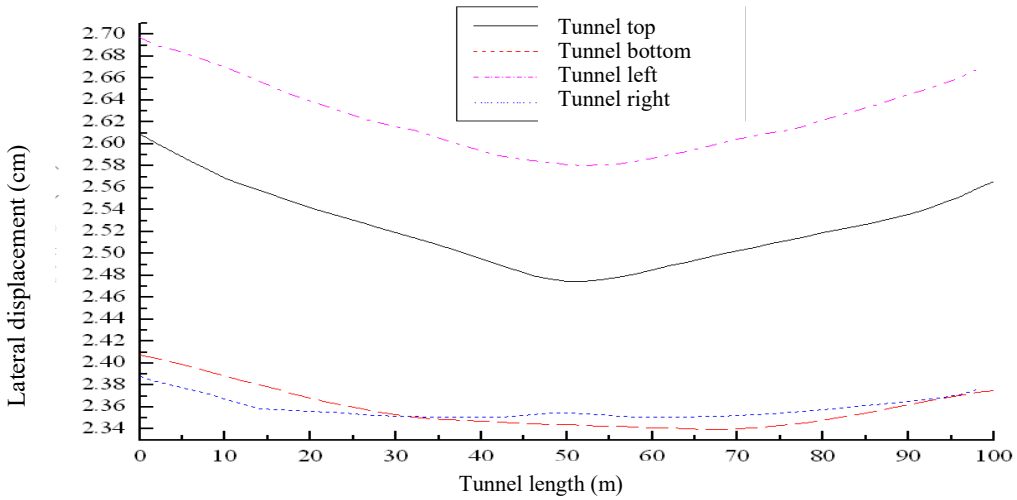

Fig. 14 Curve of the maximum lateral displacement of the tunnel along the longitudinal direction

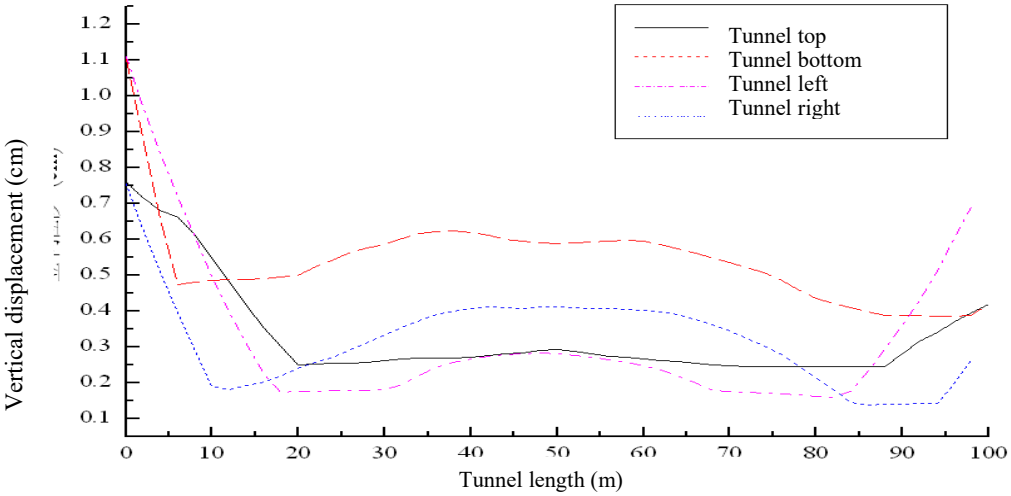

Fig.15 Change curve of vertical displacement of tunnel

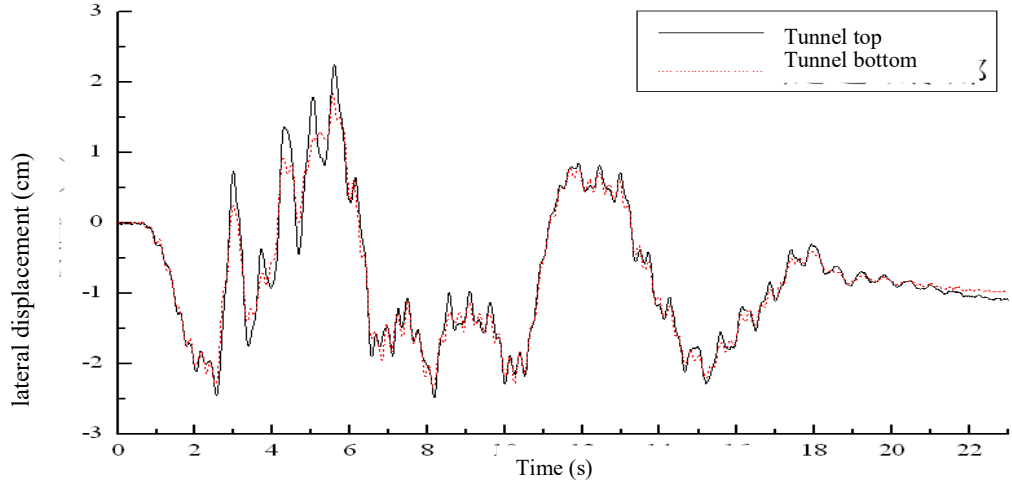

Fig.16 Curve of the horizontal and bottom displacement of the top and bottom of the longitudinal section of the tunnel

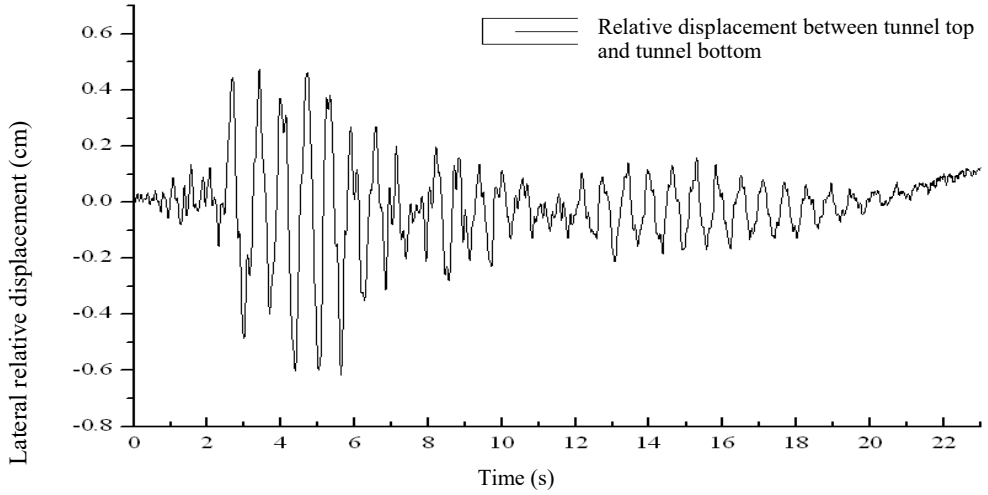

Fig.2-22 The relative displacement time course of the top and bottom of the tunnel in the longitudinal section of the tunnel

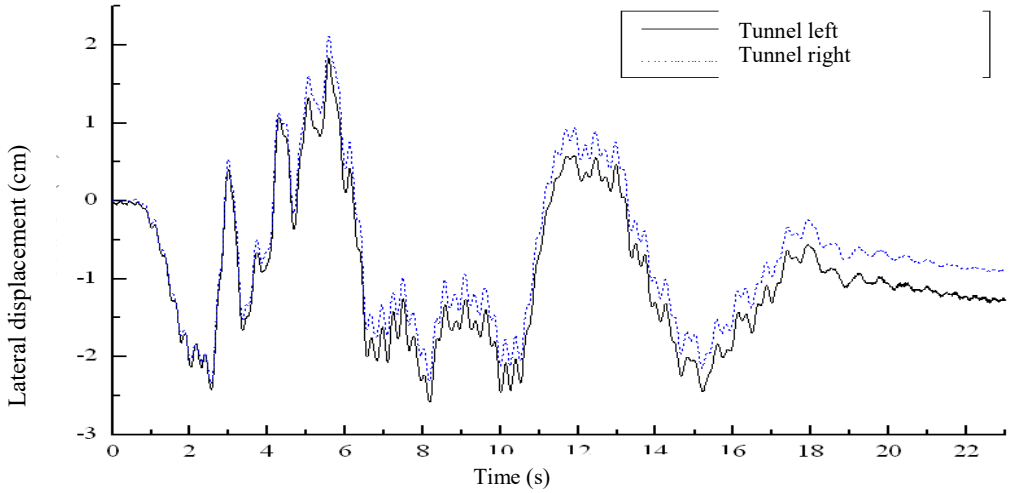

Fig.17 Time-history curve of transverse displacement of two arch trenches in longitudinal section of tunnel

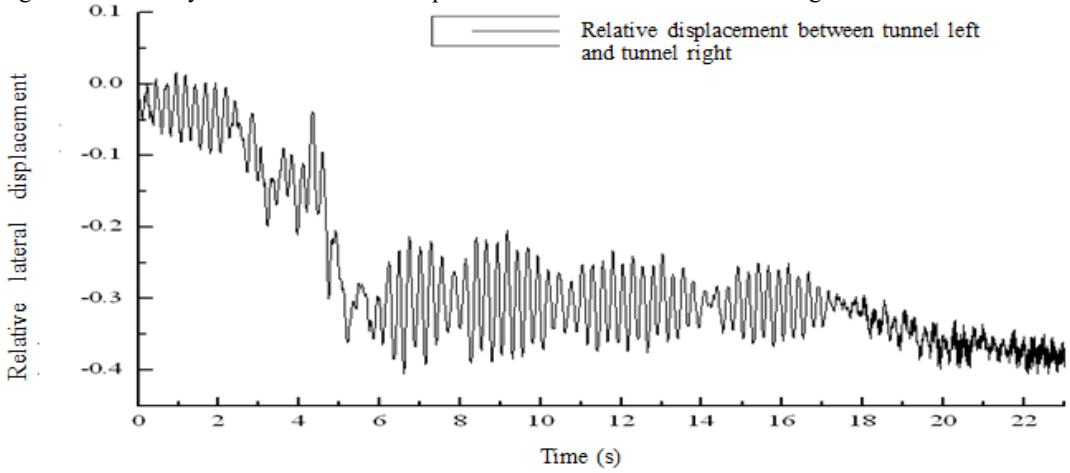

Fig.18 Time-history curve of transverse relative displacement of two arch trenches

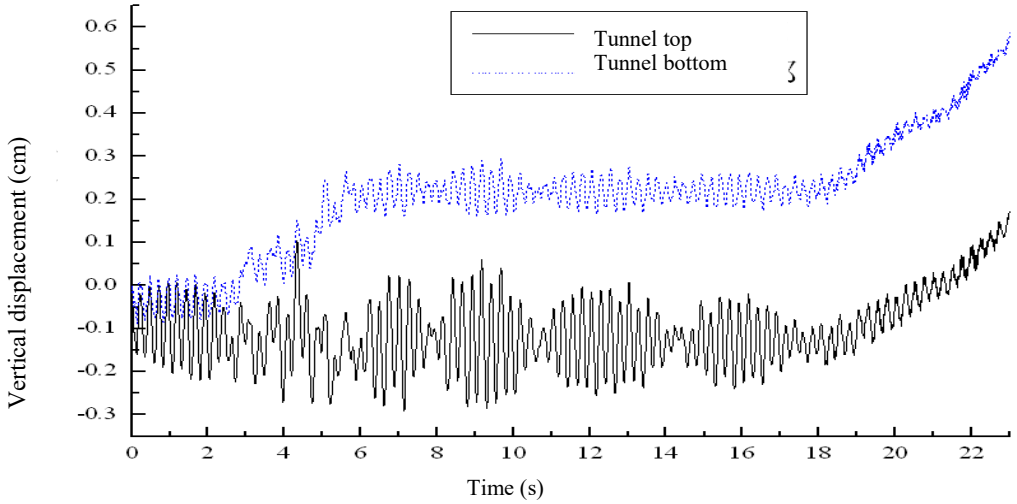

Fig.19 Time-history curve of the vertical and vertical displacement of the top and bottom of the tunnel

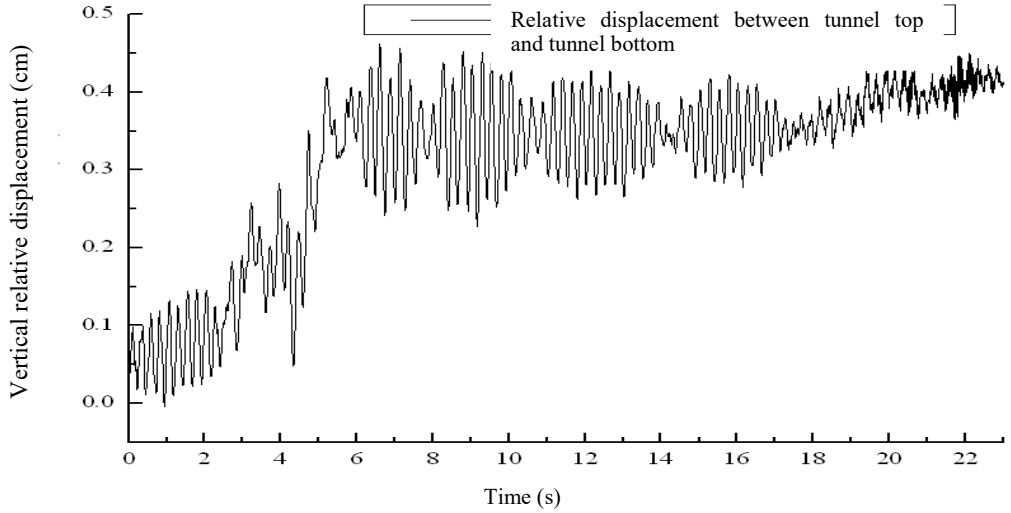

Fig.20 Time-history curve of the vertical displacement of the top and bottom of the tunnel in the longitudinal section of the tunnel

As can be seen from Figure 14-20:

1, In the transverse shear seismic wave, the lateral displacement of the tunnel is larger and the vertical displacement is smaller.

2. By the boundary conditions, the tunnel end of the larger displacement, the central displacement is smaller.

3, The maximum relative displacement of the tunnel at the top and bottom of the tunnel is 0.6cm, the maximum lateral displacement of the arch of the tunnel is 0.4cm, and the maximum vertical relative displacement of the top and bottom of the tunnel is 0.45cm.

4. Under the action of earthquake, the tunnel has some residual deformation, the relative lateral displacement of the arch of the two arch is 0.38cm, the relative vertical displacement of the bottom of the tunnel and the bottom is 0.42cm

3.4.1.3 Analysis of pore water pressure

Taking into account the symmetry of the calculation model, only the left side of the soil part of the location of the pore pressure monitoring, measuring points arranged in Figure 18, a total of 6 points, respectively, with A, B, C, D, E, F letters To represent. Where the measuring points A and D are at the same level and close to the ground, and the measuring points B and E are at the same level of height, which is the soil unit around the tunnel. The points C and F are at the same level and the depth is larger The It can be seen from Fig. 9 that the pore water pressure of the unit at the same horizontal height is almost the same. (See Figs. 19 to 21) and the

effective stress (see Figs. 22 to 24) of the soil at the measuring point A to the measuring point E, respectively.

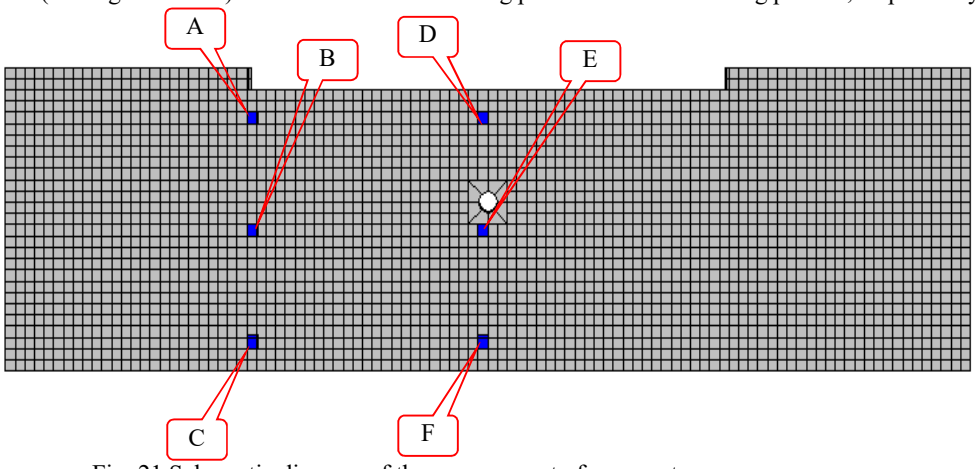

Fig. 21 Schematic diagram of the arrangement of pore water pressure

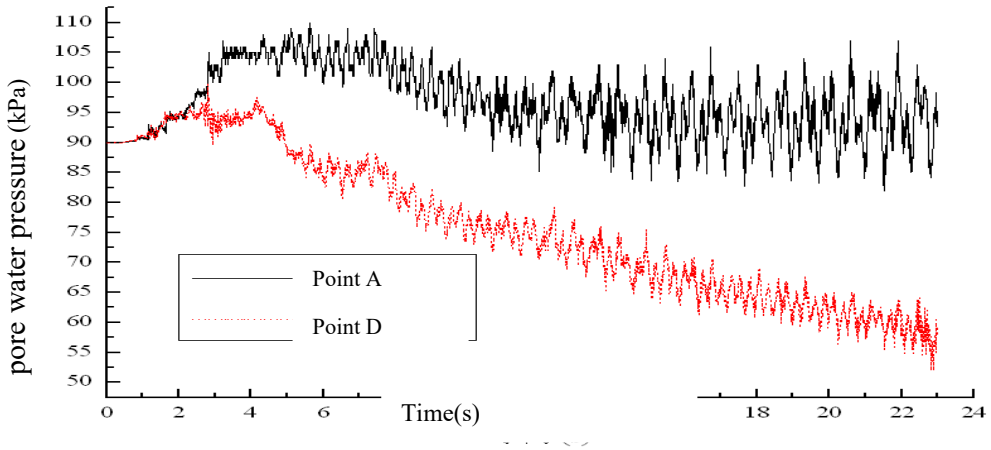

Fig.22 Time-course curve of pore water pressure at points A and D (FLAC 3D- Generated)

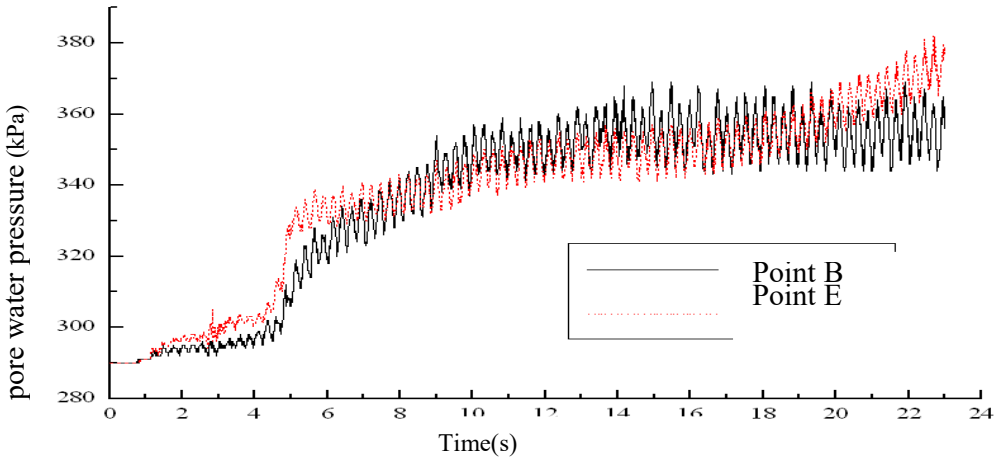

Fig.3-20 Time-course curve of pore water pressure at points B and E

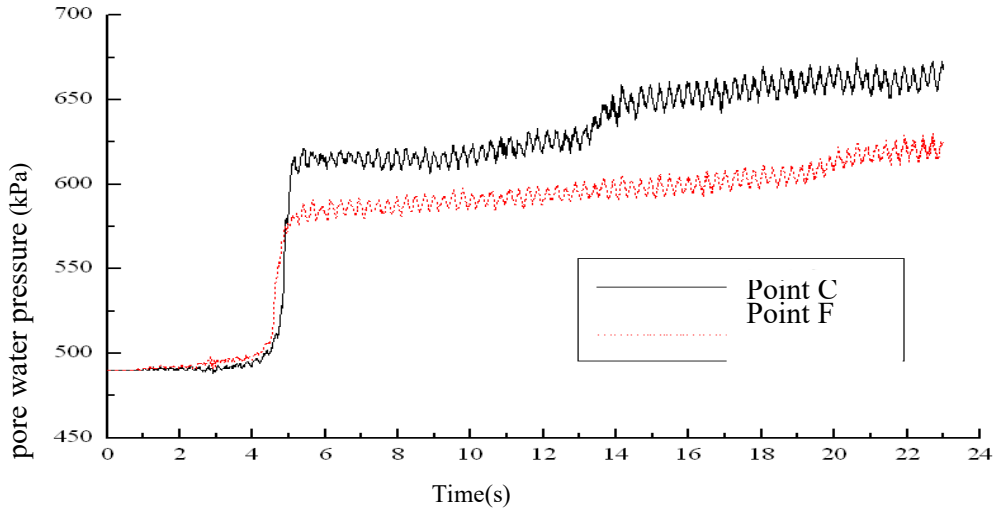

Fig.3-21 Time-history curve of pore water pressure at point C and F

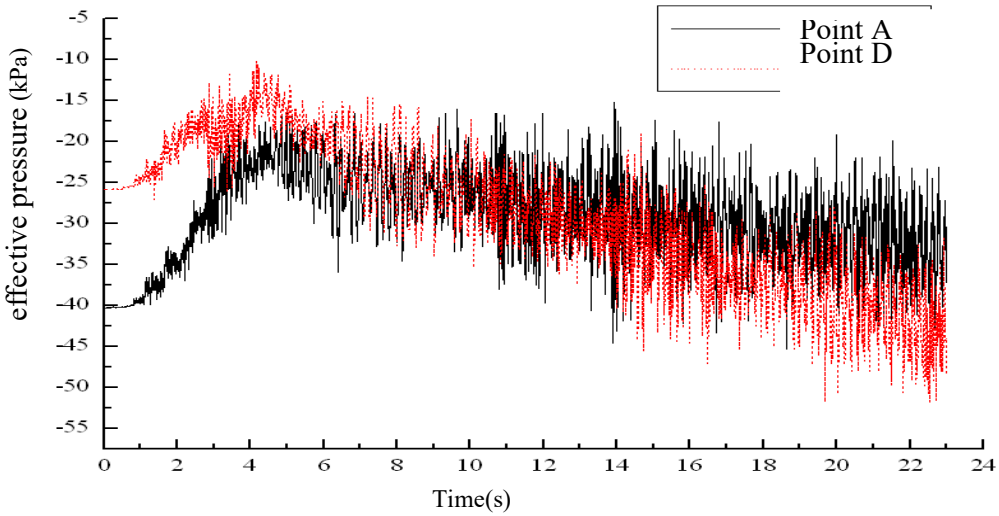

Fig.22 Time-course curve of the effective stress at points A and D

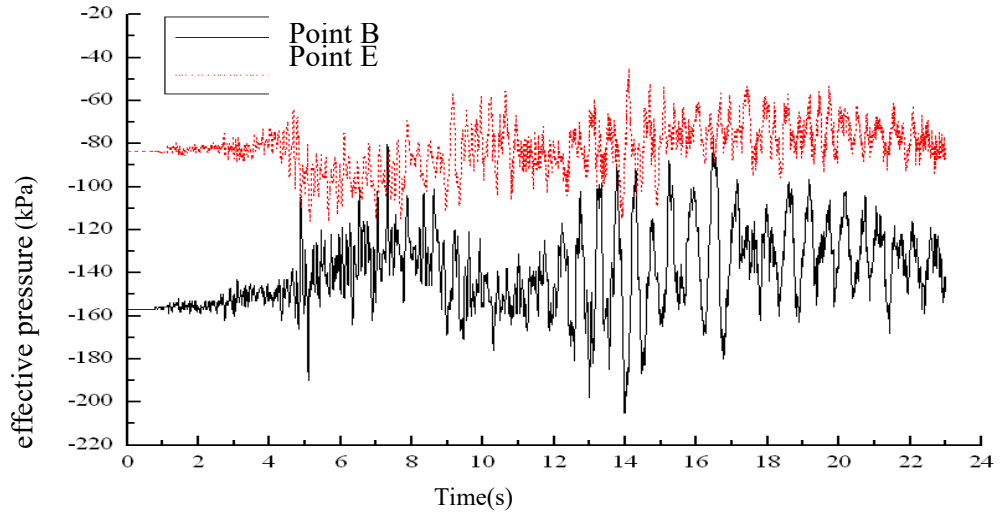

Fig.23 Time-course curve of effective stress at points B and E

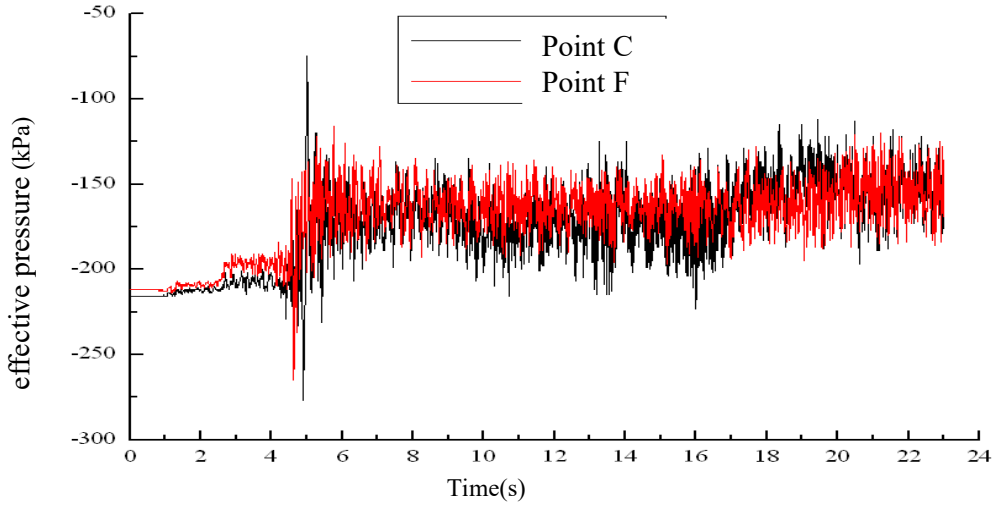

Fig.24 Time-course curve of effective stress at points C and F

As can be seen from Figure 21-24:

1, The soil at the surface is closer to the permeable boundary, and the pore water pressure is more easily dissipated. The pore water pressure of the soil is not easy to dissipate.

2, With the accumulation of pore water pressure, the effective stress decreases.

4.1 Conclusion

Bestowing to Takayuki Kishii (May 2016), for tunnels, the greater the tunneling diameter, the lower the seismic performance. Therefore, in the calculation and analysis are mainly for the larger diameter of the river tunnel, comparative analysis of the impact of groundwater, select the soil parameters are relatively weak. Therefore, the calculation and analysis is also representative, that is, Wuhan Metro subway tunnel also has resistance to middle and large earthquake seismic capacity;

Darbre, G.R. (2016), concord the fact that good job of underground building structure of urban land planning, good site selection work, try to avoid through the weak foundation, to avoid the sudden changes in the thickness of the structure of the casing to avoid the tunnel curvature should not be too small and so on the structure of the unfavorable factors. Experience in seismic design of ground structure shows that: seismic construction measures are very important. The calculation and analysis show that, the necessary seismic

construction measures can meet the seismic requirements of the underground structure during the middle and large earthquakes.

In Wuhan, there are many rivers and lakes, and the characteristics of soils are large in space, that is, there are some changes in soil parameters along the longitudinal structure, but there are no related research reports at home and abroad. However, Soil structure changes and structural changes should strengthen the underground structure of the seismic structure of the design, so that the structure has sufficient strength, but also have some ductility. (Darbre, G.R. - 2016)

Meanwhile Meek (2016), adhere to the fact that when the groundwater is not considered: In the transverse shear seismic wave, the lateral displacement of the tunnel is larger and the vertical displacement is smaller; In the transverse shear seismic wave, the transverse displacement of the top and bottom of the tunnel is the largest. More so, under the action of earthquake, the tunnel has some residual deformation. When the water is taken into account, the pore water pressure is more easily dissipated and the pore water pressure of the soil is less likely to dissipate. With the accumulation of pore water pressure, the effective stress decreases. After the end of the earthquake, the pore water pressure gradually dissipates and the effective stress increases.

At the same time, Mohammad C. Pakbaz and Akbar Yareevand (September 2005) conveyed that the rapid development of urban underground space has also brought new challenges, but also need further study which mainly include the damage mechanism of the underground structure earthquake is not clear there is no unified, perfect seismic performance evaluation method, still need further study. Wuhan geological conditions are complex, soil parameters are very uneven in spatial distribution, especially for underground tunnel structure of the shield tunnel, in the soil parameters of the tunnel structure of the lateral deformation and earthquake caused by uneven settlement and other issues are required to further study.

With the rapid development of information technology, digital underground space technology is also developing rapidly. The study of urban underground space information can grasp the basic information of urban underground space (geological conditions, spatial distribution, etc.), and the role of underground space information in earthquake relief is becoming more and more significant. Therefore, this research is also urgent to carry out. (Negro, P., Paolucci, R., Pedretti, S., Faccioli, E. - 2016)

Acknowledgements

The work was funded by Samuel Sakyi Koram (corresponding author) and Benjamin Korankye who are currently pursing their PhD studies in Solid Mechanics (PhD) and Management and Engineering (PhD) respectively at Jiangsu University, China. Particularly, we appreciate the innumerable advice and supervision of Professor Jian-Fei Lu and Wang Guobo (Associate Professor) who are tutors at Jiangsu University and Wuhan University of Technology respectively. Furthermore, we express our sincere gratitude to the Koram family for their words of encouragements and motivation.

References

[1] Japan Tunnelling Association, H. Takasaki, H Chikahisa Y. Yuasa. Planning and mapping of subsurface space in Japan, July-September 2000. Pg 287-301.
[2] Nikolai Bobylev (September, 2010). Undreground space in the Alexanderplatz area, Berlin: Research into the quantification of urban underground space use. pg 495-507.
[3] Huan-Qing Li, Aurèle Parriaux, Philippe Thalmann, Xiao-Zhao Li (September 2013). An integrated planning concept for the emerging underground urbanism: Deep City Method Part 1 concept, process and application. pg 559-568
[4] ATC (2016). Tentative Provisions for the Development of Seismic Regulations for Buildings. Applied Technology Council Report, ATC 3-06, Palo Alto, California.
[5] Xuepeng Zhang, Yujing Jiang, Satoshi Sugimoto (January 2018). Seismic damage assessment of mountain tunnel: A case study on the Tawarayama tunnel. (Tunneling) Pages 138-148, volume 71.
[6] Yu Miao, Erlei Yao, Bin Ruan, Haiyang Zhuang (2018), Seismic response of shield tunnel subjected to spatially varying earthquake ground motions (Tunneling and Underground Space Technology). Pages 216-226, Volume 77.
[7] Applied Technology Council (ATC) (2016). ATC 40: The seismic evaluation and retrofit of concrete buildings, Vol. I & II, Redwood, Palo Alto, California
[8] Building Seismic Safety Council (BSSC) (2016a). FEMA 273/274, NEHRP guidelines for the seismic rehabilitation of buildings, Vol.I–Guidelines, Vol.II – Commentary, Washington DC. Building Seismic Safety Council (BSSC) (2016b)
[9] FEMA 302/303, NEHRP recommended provisions for seismic regulations for new buildings and other structures, Vol. I – Guidelines, Vol. II – Commentary, Building Seismic Safety Council, Washington DC. CEN (2016). Eurocode 7 – Geotechnical Design Part 1: General Rules. European Committee for Standardization (CEN), Bruxelles, Belgium.

[10] Clough R.W. and Penzien, J.2016. Dynamics of Structures. McGraw-Hill Inc., New York.
[11] Takayuki Kishii (May 2016). Utillization of underground space in Japan (Tunneling and Underground Space Technology). Pages 320-323, Volume 55.
[12] Darbre, G.R. 2016. Seismic analysis of non-linearly base-isolated soil-structure interacting reactor building by way of the hybrid frequency-time-domain procedure. Earthquake Engineering and Structural Dynamics, Vol. 16, pp.725-738.
[13] Halabian, A. M. and El Naggar, M. H. 2016. Effect of foundation flexibility on seismic response of reinforced concrete TV-towers. Canadian J. of Civil Engineering, Vol. 28(3), pp.465-481.
[14] Lo Priesti, D. C. F., Pallara, O., Cavallaro, A., Maugeri, M. (2016). Nonlinear stress-strain relations of soils for cyclic loading, Proc. of XI European Conf. on Earthquake Engineering, Paris, Balkema, Abstract volume CD-ROM, 187.
[15] Meek (2016). Dynamic response of tipping core buildings. Earthquake Engineering and Structural Dynamics, Vol. 6, pp. 453-454.
[16] Mohammad C. Pakbaz, Akbar Yareevand (September 2005). Analysis of circular tunnel against earthquake loading (Tunneling and Underground Space Technology). Pages 411-417, Volume 20, Issue 5.
[17] Negro, P., Paolucci, R., Pedretti, S., Faccioli, E. (2016). Large scale soil-structure interaction experiments on sand under cyclic load. Paper No. 1191, 12th World Conference on Earthquake Engineering, Auckland, New Zealand. Institute for Catastrophic Loss Reduction 17
[18] Negro, P., Verzeletti, G., Molina, J., Pedretti, S., Lo Presti, D., Pedroni, S. (2016). Large-scale geotechnical experiments on soil-foundation interaction. Special Publication No. I.98.73, European Commission, Joint Research Center, Ispra, Italy.